Research Article | Vol. 11, No. 5 / 1 May 2021 / Optical Materials Express 1334
Optical Materials EXPRESS

AlSb as a material for high index contrast nanophotonics

HALEY C. BAUSER, DAVID R. NEEDELL, AND HARRY A. ATWATER*

Department of Applied Physics and Materials Science, California Institute of Technology, 1200 E California Blvd, Pasadena, CA 91125, USA
*haa@caltech.edu

Abstract: High contrast materials, i.e., materials with a high refractive index and low optical loss, are of wide interest for nanophotonics and metasurface designs at optical and near infrared wavelengths. We explore aluminum antimonide (AlSb) as a high contrast nanophotonic material, using the design of high contrast gratings (HCGs) for low loss dielectric mirrors as an example. The high index of refraction and low absorption coefficient of AlSb in the visible wavelength range enable designs of HCGs that can be effectively optimized to form mirrors with 93.5% reflectivity at red visible wavelengths. We detail a co-sputtering synthesis method for AlSb films, and achieve our target high index of refraction of 3.5 for 635 nm light. We also find that the high sensitivity of AlSb oxidation requires specific handling procedures in developing deposition processes to yield a near zero absorption coefficient.

1. Introduction

High refractive index materials in the visible and near infrared (NIR) wavelength range are of interest for a variety of nanophotonic applications such as visible and NIR reflectors, transmitters, vertical-cavity surface-emitting lasers, beam steering, phase changing metasurfaces, and high quality factor resonators [1–7]. Ideal materials for these applications need to have both a high index of refraction, in order to create the contrast necessary for the respective photonic phenomena, and a low absorption coefficient. A near zero absorption coefficient can enable lossless elements for high contrast nanophotonic applications. Common materials for high contrast nanophotonics include Si, amorphous Si, TiO_2, and GaP [8–10]. However, each of these semiconductor materials has limitations as high contrast metasurface elements at visible frequencies. Crystalline Si and a-Si both have high indices of refraction (n >3), but also exhibit loss in the visible wavelength range, limiting their optimal performance to the NIR [2,11]. TiO_2 is rather lossless in the visible wavelength range, but has a maximum index of refraction of 2.5, necessitating high aspect ratio resonant structures to enable the phase gradients requires by visible wavelength metasurfaces and other nanophotonic applications [10,12 13]. GaP exhibits both a high index of refraction (n>3) and near zero absorption coefficient for much of the visible and NIR, but with the limited suitable substrate materials and technically involved substrate transfer process, there exists a compelling need for high refractive index, low absorption materials that can be fabricated with common and durable processes [12]. In this paper, we explore the use of AlSb as an alternative material for utilization in high contrast nanophotonics.

One application of high contrast nanophotonics is in high contrast gratings (HCGs), structures which consist of a high index material patterned directly onto a low index substrate. HCGs have frequently been studied as an alternative to costly and angularly sensitive Bragg stack filters [1–2,14–16]. Beyond wavelength selective filters, HCGs also have applications in vertical-cavity surface-emitting lasers, high quality factor resonators, and high aperture focusing reflectors [1]. HCGs are defined as a single layer of high index material patterned at a sub-wavelength thickness onto a lower index substrate. The confinement of the impinging light allows the excitation of

#422163 https://doi.org/10.1364/OME.422163
Journal © 2021 Received 8 Feb 2021; revised 13 Mar 2021; accepted 15 Mar 2021; published 2 Apr 2021

Optical Materials EXPRESS

the transverse electric and magnetic modes of each optical element [1]. These excited modes scatter and interfere, creating sharp reflectance peaks [1–2,14–15]. These reflectance peaks can be optimized and manipulated by varying the high index material and its physical parameters of the HCG such as the shape, height, positioning, and size of the pattern. More recently, the field of HCGs has been shaped by the exploration of resonant dielectric metasurfaces for visible frequency meta-lenses [16–21]. Instead of the high index contrast producing a reflection peak, the high contrast enables the induction of a phase gradient tunable from 0 to 2π, allowing for broadband applications and cross-wavelength tunability [13,19–20,22]. Lossless HCG materials for metalenses have wide ranging applications including diagnostic imaging, unmanned automobiles, high resolution imaging optical sensors, holograms, and optical communication [20]. Therefore, AlSb HCGs could have wide ranging applications in the field of high index contrast nanophotonics.

As a specific example of an application of low loss visible wavelength HCGs achievable with AlSb, we present designs for a spectrally-selective reflector to improve the light trapping efficiency within a luminescent solar concentrator waveguide. Here we design a HCG to exhibit spectrally selective reflection around the 635 nm peak emission wavelength of high radiative efficiency CdSe/CdS quantum dots (QDs). Such QDs can be employed in solar photovoltaic applications, such as tandem luminescent solar concentrators (LSCs) [23], given the QD emission peak alignment to the indium gallium phosphide (InGaP) band edge. Previous work demonstrated the near perfect radiative characteristics of such CdSe/CdS QDs, with photoluminescence (PL) quantum yield (QY) measurements reaching up to $99.6\% \pm 0.3\%$ [24]. For LSC-specific applications, CdSe/CdS QDs are suspended in an optical waveguide coupled to embedded InGaP photovoltaic cells. The waveguide, which is most commonly a polymeric material, traps approximately 72% of the isotropic QD emission via total internal reflection [24]. In order to further trap QD PL and minimize loss through the escape cone, the QD layer is encased between two wavelength selective filters. The QDs, waveguide, InGaP photovoltaics, and filter layer define the LSC.

In applications to tandem-on-Si photovoltaics, this LSC component is then integrated on top of a silicon subcell to form a tandem photovoltaic with photoresponse across the entire solar spectrum. As shown in previous LSC research, the reflectance profile of the wavelength selective filters can significantly impact the potential power efficiency of such a device [23,25]. While Bragg stack filters can achieve high reflectance profiles in the desired emission band, such designs are costly and time intensive to fabricate, and suffer from reflectance blue-shifting with increasing angles of incidence [26–28], whereas HCGs are a more scalable and less angle sensitive than Bragg stack filters [1]. In order to find an ideal material for the high index component, we restrict our attention to materials that have both a high index of refraction and low absorption coefficient in the visible wavelength range. Materials satisfying these conditions are typically semiconductors and therefore have high absorption in the short (300-500nm) wavelength range, limiting their potential as a front reflector as this would block incident light in the QD absorption range. However, given the near-unity PLQY of such CdSe/CdS luminophores, the same restrictions on short-wavelength reflectance do not apply to the back reflector, as almost all of the light in that range will be converted by the QD layer [23,25]. AlSb is a promising material for nanophotonic applications in the visible wavelength range due to its high index of refraction ($n>3.5$) and low extinction coefficient as demonstrated in Fig. 1. It is furthermore particularly appealing for such LSC applications due to its low absorption coefficient ($k<0.006$) beyond 600nm, coinciding with the CdSe/CdS QD emission spectrum [29].

Optical Materials EXPRESS

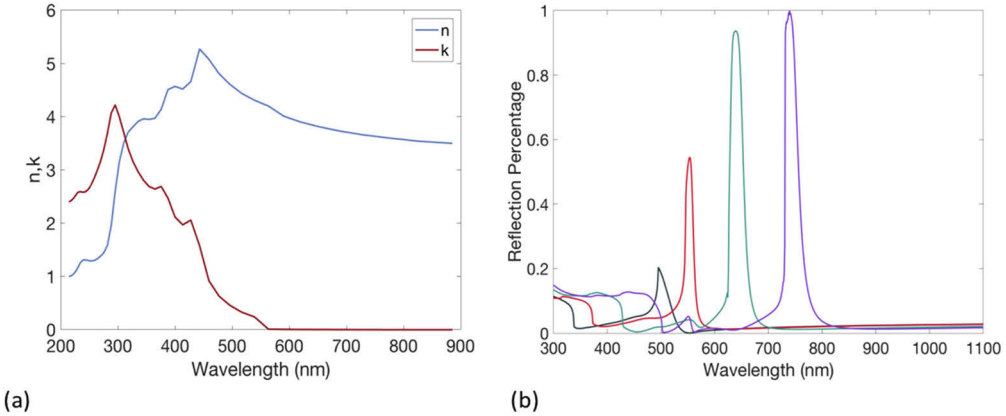

Fig. 1. In (a), the index of refraction and absorption coefficient of AlSb. The n value is 3.8 and the k value is 0.004 at 635 nm. (b) demonstration of how the reflection peak of an AlSb HCG can be optimized throughout the wavelength range of the absorption coefficient by scaling the radius, height, and pitch of the pillars.

2. LSC simulation results

In order to analyze the reflection peak of the HCGs with different geometries, we utilized finite-difference time-domain (FDTD) method electromagnetic simulations. To simulate HCG performance under the full solar spectrum, we performed broadband FDTD simulations across a wavelength range between 300 and 1100nm in order to match the solar spectrum. To fully resolve the repeating reflection modes often exhibited in HCG structures, we simulate over the maximum number of iterations for the entire duration of the FDTD resolution. If these modes are not resolved, the FDTD results can be greatly affected and ultimately inaccurate.

Given that hexagonal arrays of circular pillars allow for sharper peaks with smaller sweeping angles than square or rectangular pillar arrays [30], we focused exclusively on hexagonal arrays for the HCG design. In order to manipulate peak location, strength, and modes, we interactively

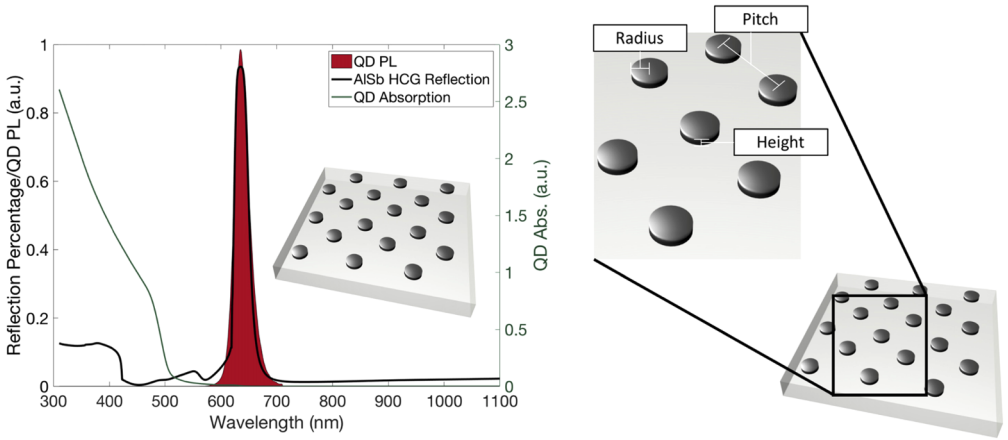

Fig. 2. Reflection peak of an AlSb high contrast grating optimized at 93.5% for the emission of CdSe/CdS quantum dots as well as a schematic of a hexagonal array of high index grating pillars. The insert shows the radius, pitch, and thickness; these are the parameters optimized to generate the given reflection peak.

Optical Materials EXPRESS

varied the pitch, height, and radius via a single parameter sweeping script. Through this sweeping optimization, we solidified an optimized pitch of 494n, an optimized height of 95 nm, and an optimized radius of 100 nm. As shown in Fig. 2, we achieved a reflection peak of 93.5% at the QD emission of 635 nm, tuned to the external quantum efficiency (EQE) of InGaP microcells. Beyond applications to InGaP-based photovoltaics, the manipulation of these modes could enable realization of such HCGs for a variety of emitter wavelengths, tuned to photovoltaic materials with different bandgaps. Figure 3 demonstrates grating tunability with InGaP, GaAs, and Si – which are all potential component materials in LSC applications [6,31–32].

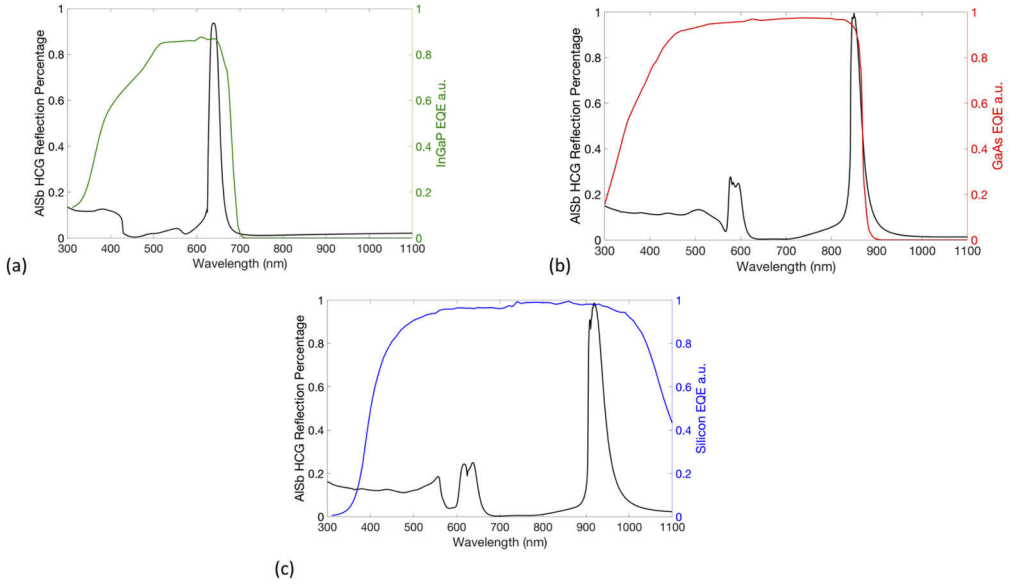

Fig. 3. Example of how by scaling the pitch, radius, and thickness of the pillars in the hexagonal array, the AlSb HCG can be tuned to a variety of photovoltaic material band edges. In (a) we show the reflection peak tuned to the band edge of InGaP. In (b) we show the reflection peak tuned to the band edge of GaAs. In (c) we show the reflection peak tuned to the near IR at the band edge of Si. The peaks in the long wavelength range show more reflection modes in the short wavelength region, but this would not be relevant as a back reflector or potentially when applied to different luminophores with different absorption profiles. The peaks are higher for the longer wavelength band edges due to the AlSb's near zero absorption beyond 700 nm.

3. Experimental results and discussion

We fabricated AlSb thin films via DC/RF co-sputtering of aluminum and antimony targets on a silicon substrate. Separate Al and Sb targets cost less, and are more readily available than an AlSb alloy target. By using separate Al/Sb targets, we maintain finer control of the thin film stoichiometry. Furthermore, co-sputtering enables a more inexpensive method for such a visible wavelength compatible, III-V HCG film fabrication as opposed to costlier methods like MOCVD [33]. We found for our sputtering system an optimized deposition rate ratio about a 3:4 of Al:Sb at 100 Watts of DC power supplied to the Al target and 50 Watts of RF power supplied to the Sb target,. While past studies have deposited films both with and without annealing [34–36], we found that annealing induces a delay in parasitic oxidation of both Al and Sb, which occurs readily without annealing. We annealed the film *in situ* directly after thin film sputtering. We heated the substrate to 550 degrees Celsius with a continuous flow of argon at 10 sccm at a

Optical Materials EXPRESS

pressure of 1mtorr to match the pressure and gas conditions of the AlSb film deposition. We find that annealing for one hour was sufficient, as any time beyond that does not contribute significant improvements to film quality or delaying of the oxidation rate.

We analyzed film composition using energy dispersive x-ray spectroscopy (EDS) and ellipsometry. While x-ray photoelectron spectroscopy (XPS) would be preferable, as it analyzes the bonding between materials, the location of the antimony and oxygen peaks makes them difficult to differentiate under analysis. The oxygen 1s peak is located approximately at 531 eV and the antimony $3d_{5/2}$ peak occurs at roughly 529 eV for AlSb. Given the sensitivity and full width half max of these energy peaks, they become extremely difficult to differentiate [37]. While possible to use the antimony $3p_{3/2}$ peak at 770 eV, we would not be able to analyze the oxidation which is crucial in the analysis of AlSb [37]. This convolution of the O_2 and Sb peaks is similarly problematic in the lower energy spectrum in EDS, therefore making definitive analysis of the ratio of oxygen, antimony, and aluminum very difficult. As a result, we found that the best way to determine film quality is through ellipsometry, which directly measures the refractive index which is the parameter of interest. Furthermore, exact X-ray analysis methods are less valuable than ellipsometry when our main figure of merit is in fact the optical properties as they are in our analysis for such HCG applications. We used ellipsometry to analyze the deposition rates conducive to AlSb optical behavior. In order to ensure accurate n,k data, we first analyzed the thin film thickness via cross-sectional SEM. If the deposition parameters result in a sample that is stoichiometric Al heavy due to a high Al deposition rate, the n and k data resemble that of aluminum. Likewise, when the stoichiometric ratio is Sb heavy, the n and k data better resemble that of antimony. Only when the the deposition rates are nearly even between the Al and the Sb do we observe semiconductor properties such as the appearance of an energy bandgap.

We found that parasitic oxidation occurred in all films, regardless of initial n,k measurements, and we therefore stored all films in inert environments between depositions and analysis. Even with this careful treatment of samples, oxidation consistently occurred and negatively impacted the n,k behavior of the films by decreasing the index and increasing the extinction coefficient. After sweeping through the respective rates of Al:Sb in the deposition process we found an optimum rate of 0.8 angstroms per second of Al and 1.05 angstroms per second of Sb, resulting in a film index of refraction of 3.5 and extinction coefficient of 0.60 at 635nm, as shown in Fig. 4.

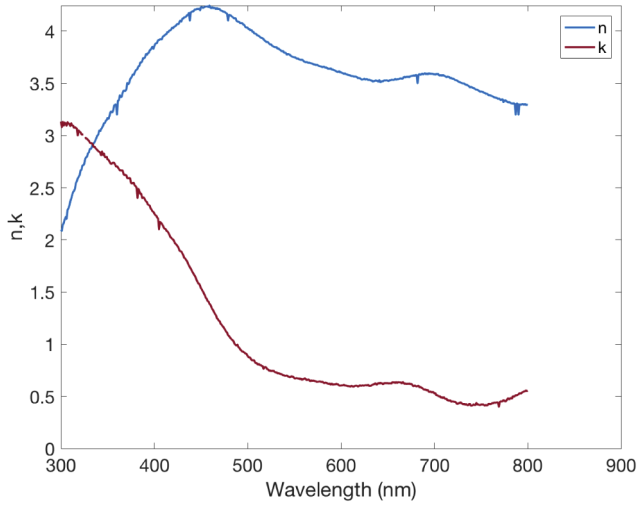

Fig. 4. Index of refraction and extinction coefficient of a fabricated AlSb thin film kept in an inert environment.

Optical Materials EXPRESS

In order to evaluate the potential of AlSb films as high contrast gratings, we incorporated films with experimentally-determined n,k data in our electromagnetic simulations. Figure 5 shows the results of this simulation using the measured n,k data. While we achieve an index of refraction n = 3.5 and, therefore, a high enough value to induce a reflection peak, the absorption coefficient is consistently too high to induce a resonant reflection peak strong enough to serve as a useful spectrally selective reflector to improve the photovoltaic conversion efficiency of LSCs.

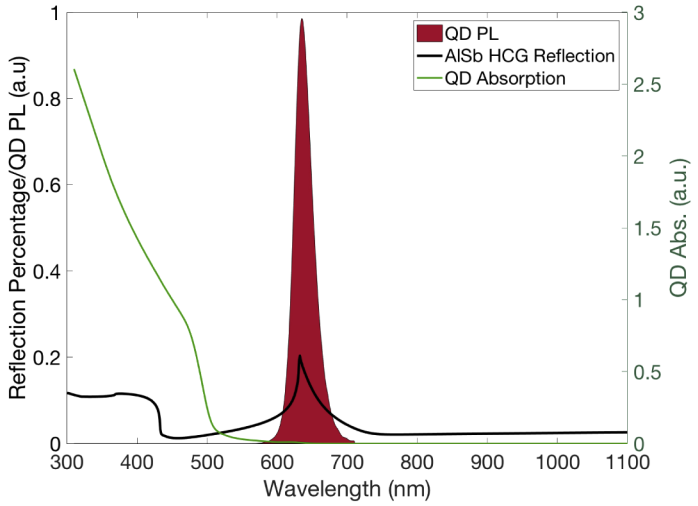

Fig. 5. FDTD Simulation of a HCG using the experimental n,k data from the deposited AlSb film. The reflection peak is 22% at 635 nm.

If the extinction coefficient could be decreased closer to the known value for single crystal AlSb films, sputtered films could be used as HCG wavelength selective reflectors. We infer that the co-sputtering process results in AlSb semiconducting thin films with defects and disorder that induce below-bandgap absorption, which is detrimental in high contrast nanophotonics applications. In order to achieve the ideal AlSb absorption performance, sputtered films must be

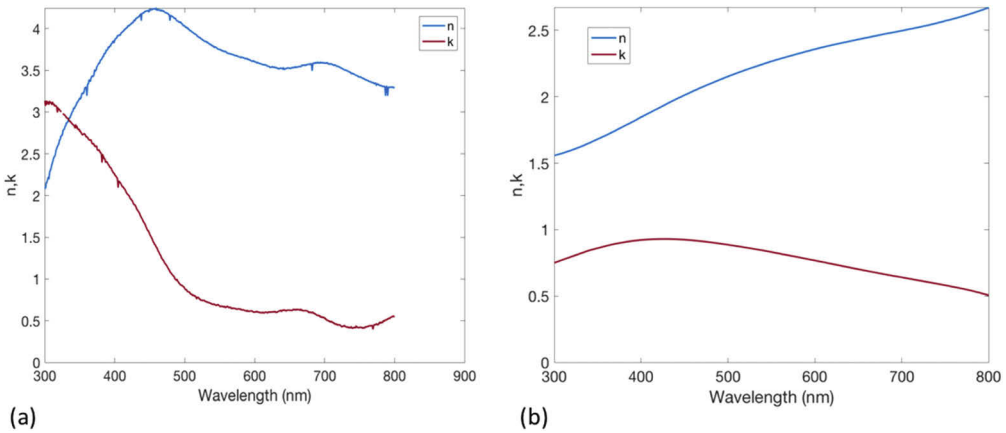

Fig. 6. (a) shows the n,k data of a thin film kept in an inert atmosphere. (b) shows the same sample after terminally oxidizing. The index of refraction decreases, and the extinction coefficient increases. This change makes the film impractical to deploy in a high contrast grating.

Optical Materials EXPRESS

more resilient to oxidation. We found that oxidation begins almost instantaneously following film exposure to a room ambient and causes the film semiconductor n,k characteristics to be severely degraded, as demonstrated in Fig. 6. Furthermore, oxidation causes an increase in film grain size that can affect device performance. The timescale required for material durability is determined first by the time required to verify the characteristics of the HCG(hours), and then ultimately by the application in deployed LSC modules(months-years). Such durability could potentially be achieved with deposition methods such as MOCVD or sputtering with forming gas or hydrogen, that are more typically utilized in III-V thin film fabrication [6,34–35,38], following by deposition of an environment barrier coating to inhibit oxidation. These methods could improve the crystalline quality of AlSb material and therefore increase the material durability with respect to oxidation.

4. Conclusions

AlSb exhibits a high index of refraction and near zero absorption coefficient in the visible and NIR, making it an interesting material to explore for applications in high contrast nanophotonics. In this work, we have demonstrated that an AlSb high contrast grating with ideal complex refractive index can be used as a spectrally-selective mirror to improve the light trapping efficiency in luminescent solar concentrator waveguides. Though our work specifically focused on the optimization of an HCG for reflecting emission by CdSe/CdS quantum dot luminophores tuned to the band edge of a InGaP photovoltaic cell, we additionally demonstrated the versatility of HCG design for design of spectrally selective reflectors at longer wavelengths, matched to the band edges of GaAs and Si photovoltaic cells, illustrating the potential of AlSb as an HCG reflector in the visible and near infrared wavelength range. We found that AlSb semiconducting thin films fabricated by sputter deposition exhibit a high absorption coefficient that diminishes reflectance of HCGs. Rapid parasitic oxidation is the factor currently limiting in the deployment of AlSb HCG reflectors fabricated by sputter deposition. Different deposition methods such as MOCVD or sputtering with a forming gas ambient may be able to mitigate or eliminate this parasitic absorption. If so, future AlSb films could have extensive application in high contrast nanophotonics, including photovoltaic structures such as luminescent solar concentrators.

Funding. Space Solar Power Project; Advanced Research Projects Agency - Energy (DE-AR0000627).

Acknowledgments. This work was supported by the Space Solar Power project and the U.S. Department of Energy, Advanced Research Projects Agency for Energy under Grant DE-AR0000627. Fabrication and analysis support and infrastructure was provided by the Kavli Nanoscience Institute at Caltech.

Disclosures. The authors declare that there are no conflicts of interest related to this article.

Supplemental document. See Supplement 1 for supporting content.

References

1. C. J. Chang-Hasnain and W. Yang, "High-contrast gratings for integrated optoelectronics," Adv. Opt. Photonics **4**(3), 379–440 (2012).
2. R. C. Ng, J. C. Garcia, J. R. Greer, and K. R. Fountaine, "Polarization-independent, narrowband, near-IR spectral filters via guided mode resonances in ultrathin a-Si nanopillar arrays," ACS Photonics **6**(2), 265–271 (2019).
3. J. K. S. Poon, "Integrated ultra-low-loss resonator on a chip," Nat. Photonics **12**(5), 255–256 (2018).
4. Z. Zhou, J. Li, R. Su, B. Yao, H. Fang, K. Li, L. Zhou, J. Liu, D. Stellinga, C. P. Reardon, T. F. Krauss, and X. Wang, "Efficient silicon metasurfaces for visible light," ACS Photonics **4**(3), 544–551 (2017).
5. P. C. Wu, J. Chen, C. Yin, Y. Lai, T. L. Chung, C. Y. Liao, B. H. Chen, K. Lee, C. Chuang, C. Wang, and D. P. Tsai, "Visible metasurfaces for on-chip polarimetry," ACS Photonics **5**(7), 2568–2573 (2018).
6. R. A. Aoni, M. Rahmani, L. Xu, K. Z. Kamali, A. Komar, J. Yan, D. Neshev, and A. E. Miroschichenko, "High-efficiency visible light manipulation using dielectric metasurfaces," Sci. Rep. **9**(1), 6510 (2019).
7. S. Gao, S. Lee, E. Kim, and D. Choi, "Vertically integrated visible and near-infrared metasurfaces enabling an ultra-broadband and highly angle-resolved anomalous reflection," Nanoscale **10**(26), 12453–12460 (2018).
8. H. Emmer, C. T. Chen, R. Saive, D. Friedrich, Y. Horie, A. Arbabi, A. Faraon, and H. A. Atwater, "Fabrication of single crystal gallium phosphide thin films on glass," Sci. Rep. **7**(1), 4643 (2017).

Optical Materials EXPRESS

9. D. O'Mahony, M. N. Hossain, J. Justice, E. Pelucchi, A. O'riordan, B. Roycroft, and B. Corbett, "High index contrast optical platform using gallium phosphide on sapphire: an alternative to SOI?" Proc. SPIE **8431**, 84311H (2012).
10. Y. Wu, W. Yang, Y. Fan, Q. Song, and S. Xiao, "TiO_2 metasurfaces: from visible planar photonics to photochemistry," Sci. Adv. **5**(11), eaax0939 (2019).
11. D. E. Aspnes and A. A. Studna, "Dielectric functions and optical parameters of Si, Ge, GaP, GaAs, GaSb, InP, InAs, and InSb from 1.5 to 6.0 eV," Phys. Rev. B **27**(2), 985–1009 (1983).
12. N. M. Estakhri, V. Neder, M. W. Knight, A. Polman, and A. Alu, "Visible light, wide-angle graded metasurface for back reflection," ACS Photonics **4**(2), 228–235 (2017).
13. X. Buet, D. E. Belharet, F. Lozes-Dupuy, A. Monmayrant, and O. Gauthier-Lafaye, "High angular tolerance and reflectivity with narrow bandwidth cavity-resonator-integrated guided-mode resonance filter," Opt. Express **20**(8), 9322 (2012).
14. M. Khorasaninejad, W. T. Chen, R. C. Devlin, J. Oh, A. Y. Zhu, and F. Capasso, "Metalenses at visible wavelengths: diffraction-limited focusing and subwavelength resolution imaging," Science **352**(6290), 1190–1194 (2016).
15. B. Cheong, O. N. Prudnikov, F. Cho, H. Kim, J. Yu, Y. Cho, H. Choi, and S. T. Shin, "High angular tolerant color filter using subwavelength grating," Appl. Phys. Lett. **94**(21), 213104 (2009).
16. M. Niraula, J. W. Yoon, and R. Magnusson, "Single-layer optical bandpass filter technology," Opt. Lett. **40**(21), 5062–5065 (2015).
17. W. Yang, S. Xiao, Q. Song, Y. Liu, Y. Wu, S. Wang, J. Yu, J. Han, and D. P. Tsai, "All-dielectric metasurface for high performance structural color," Nat. Commun. **11**(1), 1864 (2020).
18. P. Camayad-Munoz, C. Ballew, G. Roberst, and A. Faraon, "Multifunctional volumetric meta-optics for color and polarization image sensors," Optica **7**(4), 280–283 (2020).
19. H. Sroor, Y. Huang, B. Sephton, D. Naidoo, A. Valles, V. Ginis, C. Qiu, A. Ambrosio, F. Capasso, and A. Forbes, "High-purity orbital angular momentum states from a visible metasurface laser," Nat. Photonics **14**(8), 498–503 (2020).
20. M. L. Tseng, H. Hsiao, C. H. Chu, M. K. Chen, G. Sun, A. Liu, and D. P. Tsai, "Metalenses: advances and applications," Adv. Opt. Mater. **6**(18), 1800554 (2018).
21. R. J. Lin, V. Su, S. Wang, M. K. Chen, T. L. Chung, Y. H. Chen, H. Y. Kuo, J. Chen, J. Chen, Y. Huang, J. Wang, C. H. Chu, P. C. Wu, T. Li, Z. Wang, S. Zhu, and D. P. Tsai, "Achromatic metalens array for full-colour light-field imaging," Nat. Nanotechnol. **14**(3), 227–231 (2019).
22. J. Xu, M. Cua, E. H. Zhou, Y. Horie, A. Faraon, and C. Yang, "Wide-angular-range and high-resolution beam steering by a metasurface-coupled phased array," Opt. Lett. **43**(21), 5255–5258 (2018).
23. D. R. Needell, O. Ilic, C. R. Bukowsky, Z. Nett, L. Xu, J. He, H. Bauser, B. G. Lee, J. F. Geisz, R. G. Nuzzo, A. P. Alivisatos, and H. A. Atwater, "Design criteria for micro-optical tandem luminescent solar concentrators," IEEE J. Photovoltaics **8**(6), 1560–1567 (2018).
24. D. A. Hanifi, N. D. Bronstein, B. A. Koscher, Z. Nett, J. K. Swabeck, K. Takano, A. M. Schwartzberg, L. Maserati, K. Vandewal, Y. van de Burgt, A. Salleo, and A. P. Alivisatos, "Redefining near-unity luminescence in quantum dots with photothermal threshold quantum yield," Science **363**(6432), 1199–1202 (2019).
25. H. Bauser, D. R. Needell, C. R. Bukowsky, O. Ilic, Z. Nett, B. Lee, J. F. Geisz, A. P. Alivisatos, and H. A. Atwater,"Metasurfaces as wavelength selevtice mirrors in tandem luminescent solar concentrators," *PVSC45th Conference Proceedings* (2018)
26. J. W. Leem, X. Guan, and J. S. Yu, "Tunable distributed Bragg reflectors with wideangle and broadband high-reflectivity using nanoporous/dense titanium dioxide film stacks for visible wavelength applications," Opt. Express **22**(15), 18519–18526 (2014).
27. D. K. G. de Boer, D. J. Broer, M. G. Debije, W. Keur, A. Meijerink, C. R. Ronda, and P. P. C. Verbunt, "Progress in phosphors and filters for luminescent solar concentrators," Opt. Express **20**(S3), A395–A405 (2012).
28. D. K. G. de Boer, "Optimizing wavelength-selective filters for luminescent solar concentrators," Sol. Energy **7725**, 77250Q (2010).
29. S. Zollner, C. Lin, E. Schonherr, A. Bohringer, and M. Cardona, "The dielectric function of AlSb from 1.4 to 5.8 eV determined by spectroscopic ellipsometry," J. Appl. Phys. **66**(1), 383–387 (1989).
30. S. Darbe and H. A. Atwater, "Resonant dielectric high-contrast gratings as spectrum splitting optical elements for ultrahigh efficiency (>50%) photovoltaics," *PVSC, 42nd Conference Proceedings* 2015.
31. M. A. Green, Y. Hishikawa, W. Warta, E. D. Dunlop, D. H. Levi, J. Hohl-Ebinger, and A. W. Ho-Baillie, "Solar cell efficiency tables (version 50)," Prog. Photovolt. Res. Appl. **25**(7), 668–676 (2017).
32. S. Theingi, D. R. Needell, H. Bauser, M. Phelan, W. Nemeth, D. Findley, H. Su, B. Koscher, Z. Nett, O. Ilic, C. R. Bukowsky, R. G. Nuzzo, A. P Alivisatos, J. F. Geisz, P. Stradins, and H. A. Atwater, "Luminescent solar concentrator tandem-on-silicon with above 700 mV passivated contace silicon bottom cell," *PVSC, 46th Conference Proceedings* (2019)
33. K. A. Horowitz, T. Remo, B. Smith, and A. Ptak, "Techno-economic analysis and cost reduction roadmap for III-V solar cells," Golden, CO: National Renewable Energy Laboratory. NREL/TP-6A20-72103. (2018)
34. R. Giulian, D. J. Manzo, J. B. Salazar, W. Just, A. M. H. de Andrade, J. R. Schoffen, L. A. B. Niekraszewicz, J. F. Dias, and F. Bernardi, "Structural and electronic characterization of antimonide films made by magnetron sputtering," J. Phys. D: Appl. Phys. **50**(7), 075106 (2017).

Optical Materials EXPRESS

35. W. Chen, L. Feng, Z. Lei, J. Zhang, F. Yao, W. Cai, Y. Cai, W. Li, L. Wu, B. Li, and J. Zheng, "AlSb thin films prepared by DC magnetron sputtering and annealing," Int. J. Mod. Phys. B **22**(14), 2275–2283 (2008).
36. H. Zheng, W. Li-Li, L. Bing, H. Xia, H. Jian-Xiong, F. Liang-Huan, L. Wei, Z. Jing-Quan, and C. Yap-Ping, "The electrical, optical properties of AlSb polycrystalline thin films deposited by magnetron co-sputtering without annealing," Chin. Phys. B **19**(12), 127501 (2010).
37. J. F. Moulder, *Handbook of X-Ray Photoelectron Spectroscopy: A Reference Book of Standard Spectra for Identification and Interpretation of XPS Data* (Perkin-Elmer Corporation, 1992).
38. J. F. Geisz and D. J. Friedman, "III-N-V semiconductors for solar photovoltaics applications," Semicond. Sci. Technol. **17**(8), 769–777 (2002).